Behavioral/Cognitive

Load Dependence of β and γ Oscillations Predicts Individual Capacity of Visual Attention

Sateri Rouhinen,[1,2] Jonatan Panula,[1] J. Matias Palva,[1] and Satu Palva[1]

[1]Neuroscience Center, University of Helsinki, 00014 Helsinki, Finland, and [2]BioMag Laboratory, HUS Medical Imaging Center, Helsinki University Central Hospital, 00029 Helsinki, Finland

Human capability to concurrently attend and perceive multiple visual objects has a limited and individual capacity of 2–4 objects. Neuronal mechanisms that support the perception of multiple objects and underlie these attentional capacity limits have remained unclear. We investigated the role of neuronal oscillations in multiobject visual perception and in limiting the attentional capacity. To this end, we used parametric multiobject tracking tasks, MEG and EEG recordings, and data-driven source-space analyses to localize the neuronal substrates of task performance. Three lines of evidence suggested a mechanistic role for neuronal oscillations in multiobject attention. First, oscillation amplitudes preceding target events were distinct for subsequently detected and undetected targets and also predicted reaction times to the target events. Second, suppression of θ to low-β (<20 Hz) and strengthening of high-β to γ (20–90 Hz) oscillations in frontoparietal and visual regions were correlated with attentional load. Third, the load-dependent strengthening of γ (30–90 Hz) band oscillations in lateral prefrontal, posterior parietal, and visual cortices predicted interindividual variability in attentional capacity. A progressive recruitment of γ oscillations in sensory, attentional, and executive networks is thus directly correlated with multiobject attentional demands and, in particular, with the individual capability to consciously attend and perceive multiple visual objects concurrently. These data support the hypothesis that γ oscillations contribute both to neuronal object representations and to attentional and executive processing.

Key words: **MEG; EEG; attention; oscillation; synchrony**

Introduction

Humans can consciously attend only up to four visual objects. The neuronal mechanisms underlying this capacity limit have remained unclear. The capacity of sustained attention during continuous perceptual processing has been assessed with multiobject tracking (MOT) tasks in which subjects track a parametrically variable number of moving visual objects (Pylyshyn and Storm, 1988; Oksama and Hyönä, 2004; Bettencourt et al., 2011). fMRI studies with MOT tasks have shown that, in lateral prefrontal (LPFC) and posterior parietal (PPC) cortices, the fMRI signal is positively correlated with the number of attended objects (Culham et al., 1998; Jovicich et al., 2001), suggesting that the increasing attentional load is paralleled by progressive engagement of these attention- and task-control systems. Both attention (Pylyshyn and Storm, 1988; Treisman, 2006; Bettencourt et al., 2011) and working memory (WM) (Luck and Vogel, 1997; Cowan et al., 2005) have a highly individual capacity of $\sim 3 \pm 1$ objects, and these capacities are correlated (Oksama and Hyönä, 2004). Indeed, fMRI studies indicate a role for the LPFC-PPC network also in multiobject WM maintenance and capacity (Linden et al., 2003; Todd and Marois, 2004; Xu and Chun, 2009). Furthermore, EEG studies show that similar slow potential shifts are correlated with the number of attended items during visual tracking (Drew and Vogel, 2008) and maintained in visual WM (Vogel and Machizawa, 2004). These data imply that the maintenance of multiple objects in the focus of attention or in WM could rely on similar neuronal mechanisms.

Synchronization of neuronal activity in β (15–30 Hz) and γ (30–90 Hz) frequency bands gives rise to transient neuronal assemblies that may through relational coding beget both coordination of attentional interactions and feature binding for neuronal representations of perceptual objects (Singer, 1999; Womelsdorf and Fries, 2007). Allocation of spatial attention strengthens β and γ synchronization among visual regions, PPC, and LPFC in monkey local field potential recordings (Womelsdorf et al., 2006; Gregoriou et al., 2009; Buschman and Miller, 2010; Bosman et al., 2012). In humans, spatial attention modulates the amplitude and hence local synchronization of γ oscillations in sensor-level analyses of EEG (Gruber et al., 1999) and MEG (Wyart and Tallon-Baudry, 2008). In source-reconstructed MEG, spatial attention to motion stimuli is associated with strengthened γ oscillations in posterior contralateral brain regions (Siegel et al., 2008). α-Frequency-band (8–14 Hz) oscillations may also support attention, albeit with complementary functional roles (Klimesch et al., 2007; Palva and Palva, 2007; Saalmann et al., 2012). The functional roles of α- and γ-band

Received April 19, 2013; revised Oct. 21, 2013; accepted Oct. 29, 2013.

Author contributions: J.M.P. and S.P. designed research; S.R. performed research; S.R. and J.P. analyzed data; S.R., J.M.P., and S.P. wrote the paper.

This work was supported by the Academy of Finland (SA 1126967, 266402, 253130, and 256472) and by the Helsinki University Research Funds.

The authors declare no competing financial interests.

Correspondence should be addressed to Dr. Satu Palva, Neuroscience Center, P.O. Box 56, University of Helsinki, 00014 Helsinki, Finland. E-mail: satu.palva@helsinki.fi.

DOI:10.1523/JNEUROSCI.1666-13.2013

 0270-6474/13/3319023-11$15.00/0

oscillations in multiobject attention have, however, remained unclear.

Load-dependent strengthening of γ amplitude predicts both individual WM capacity limits (Palva et al., 2011) and the number of items in WM (Roux et al., 2012), which suggests that these oscillations could play a role also in multiobject attention. We used source-reconstructed MEG/EEG to identify the cortical structures underlying the attention-dependent modulations in oscillation amplitudes and to ask whether cortical oscillations predict attentional capacity limits and behavioral performance during sustained multiobject attention.

Materials and Methods

Participants, task, and stimuli. Concurrent MEG and EEG (MEG/EEG) were recorded from 19 subjects (8 females; mean ± SD age, 26 ± 3.5 years). In Task 1 (T1), the subjects' task was to attend and track one, two, three, or four seminaturally moving discs with a blank sector pointing to the direction of the motion and to detect brief (~100 ms) changes in the sector size (see Fig. 1*B*). These shape changes were thus so brief that the subjects did not have time to make a saccade to the object or to "make a second glimpse" to detect the target event. Size of the discs was 0.8 degrees and the vertical size of the display 10 degrees. Background luminance was 33 cd/m^2 and stimuli luminance was 270 cd/m^2 (Minolta LS-110 luminance meter). The objects moved as per kinematic law of motion, which is faster when they are going straighter and slower the sharper they turn (Dayan et al., 2007) so that velocity V was proportional to $R^{1/3}$, where R is the radius of the local curvature of the path. The objects were not allowed to collide with each other or with the screen borders. Data for each attentional-load condition (the number of attended objects) were acquired continuously in trials lasting 45 s followed by breaks of 16 s. Each trial contained 16 target events with an interstimulus interval ranging from 0.7 to 5 s. One measurement block comprised of five trials, and the order of conditions in each block was randomized across subjects. In the second task (T2), the task was otherwise the same, but the number of moving discs was constantly held at four, and the subject was instructed to attend to the pink and to ignore the yellow discs. The number of the to-be attended discs varied from one to four in separate trials as in T1. A total of 160 target events in 10 trials were presented for each of the four attentional-load conditions in both T1 and T2 (for task dynamics and analysis window, see Fig. 1*I*). After the rejection of target events contaminated by blinks or large eye movements, an average of 133 ± 17 (SD) and 127 ± 29 target events remained in each condition in T1 and T2, respectively. For each task and subject, the minimum number of target events across the four conditions was used to obtain an equal amount of events across the conditions. This study was approved by the ethical committee of Helsinki University Central hospital and was performed according to the Declaration of Helsinki. Written informed consent was obtained from each subject before the experiment.

Data acquisition and preprocessing. The 366-channel MEG/EEG data were recorded with 204 planar gradiometers, 102 magnetometers, and 60 nose-referenced-EEG electrodes (Elekta Neuromag) at 600 Hz sampling rate. Thumb-twitch responses were recorded with electromyography of abductor/flexor pollicis brevis and detected with an automatic algorithm. Electro-oculogram (EOG) was used to detect ocular artifacts, and trials with the electro-oculogram signal exceeding 50 μV were excluded from further analysis. MaxFilter software (Elekta Neuromag) was used to suppress extracranial noise and to colocalize the signal space data from different recording sessions and subjects. Independent component analysis (ICA) was used to remove components from unfiltered data that correlated with EOG, heart-beat estimated from MEG magnetometers, or had both a very spiked spatial distribution and a non–power-law distributed spectrum using the FieldTrip MATLAB toolbox (MathWorks). These ICA components were manually removed, and then the raw data were reconstructed from the remaining components. For cortical surface reconstructions, we recorded T1-weighted (MP-RAGE) anatomical MR images at a $\leq 1 \times 1 \times 1$ mm resolution with a 1.5 T MRI scanner (Siemens).

Behavioral performance. Target events that were followed by a response within the time window from 0.25 to 0.7 s were classified as "detected." Hit rate (HR) was defined as the detection accuracy (i.e., as the fraction of detected target events from all presented events). Reaction time (RT) was given by the time from the target onset to the onset of the EMG activity of the abductor/flexor pollicis brevis and corresponding to the thumb-twitch responses.

The overall magnitude and the proportion of fast (saccadic) eye movements were estimated from EOG using the same trials as were used in other analyses. Eye motion index was defined as the mean amplitude of broad-band (1–120 Hz) filtered vertical and horizontal EOG. Saccadic motion index was obtained by derivating the filtered EOG signals and taking the mean absolute value of these derivatives.

Source analysis, surface parcellations, and filtering. The MEG/EEG source reconstruction, filtering, and statistics were performed largely as earlier (Palva et al., 2010, 2011). Briefly, we used FreeSurfer software (http://surfer.nmr.mgh.harvard.edu/) for automatic volumetric segmentation of the MRI data, surface reconstruction, flattening, cortical parcellation, and labeling with the Freesurfer/Destrieux atlas (Dale et al., 1999; Fischl et al., 1999, 2002). We used MNE software (http://www.nmr.mgh.harvard.edu/martinos/userInfo/data/sofMNE.php) to create three-layer boundary element conductivity models and cortically constrained source models for the MEG/EEG-MRI colocalization and for the preparation of the forward and inverse operators (Hämäläinen and Sarvas, 1989; Hämäläinen and Ilmoniemi, 1994).

We filtered each channel of the single-trial MEG/EEG time-series data into 31 frequency bands (f, $f = 3 \ldots 90$ Hz) with Morlet wavelets and prepared inverse operators separately for each wavelet filter frequency. For cortex-wide mapping of amplitude dynamics, we collapsed the 6000–8000 source vertex time series of single-trial inverse estimates into time series of cortical parcels in a 400-parcel parcellation. This collapsing was done so that the time series of each parcel was obtained as a weighted average of the source vertex time series. We obtained the weights so that they maximized parcel time-series reconstruction fidelity. For this optimization, we first simulated for each source parcel a white noise time series that was shared by all vertices within the parcel. The vertex time series were forward and inverse modeled and collapsed to obtain modeled parcel time series. We defined fidelity, f, as the phase correlation between the original and modeled time series of a parcel, and infidelity, i, as the phase correlation between the modeled parcel time series and the original time series of other parcels. The vertex weights were set so that the selection criterion $0.7f + 0.3(1 - i)$ was maximized. This optimization approach was applied to an anatomic parcellation of 400 parcels that were derived from the Destrieux atlas (Fischl et al., 2002) by iteratively splitting the parcels that had the largest size in the subject population along the axis (anterior–posterior, lateral–medial, ventral–dorsal) with largest mean variance (Palva et al., 2010). These fidelity-optimized parcellations supported accurate reconstruction of neuronal activity in superficial cortical structures ($f > 0.4$), but the activity in some deep and/or medial cortical structures were less accurately reconstructed ($f < 0.2$).

Data analysis and group statistics. The single-trial inverse estimates in the 400-parcel parcellation were collapsed across target events for cortex-wide mapping of ongoing amplitude dynamics. We estimated the averaged event-related amplitude envelopes (Tallon-Baudry et al., 1996; Palva et al., 2005) for 500 ms time windows preceding the target events (-0.7 to -0.2 s) and free of >50 μV EOG events (blinks and large saccades). For group statistics, the trial-averaged amplitude data obtained in the 400-parcel analysis parcellations that were common across subjects were obtained by splitting the 150 labels of the Destrieux atlas in FreeSurfer as earlier (Palva et al., 2010, 2011). Group statistics of oscillations amplitudes were then computed across subjects for each experimental contrast, frequency band, and anatomic parcel.

To elucidate pretarget neuronal correlates of target detection, we compared target events with detected targets (hits) against target events with undetected targets (misses) by collapsing for hits and misses equal amounts of trials from 2- and 3-target conditions and by using t tests with significance threshold of $p < 0.05$ (see Fig. 2). To assess whether the RTs were correlated with oscillation amplitude modulations, we collapsed

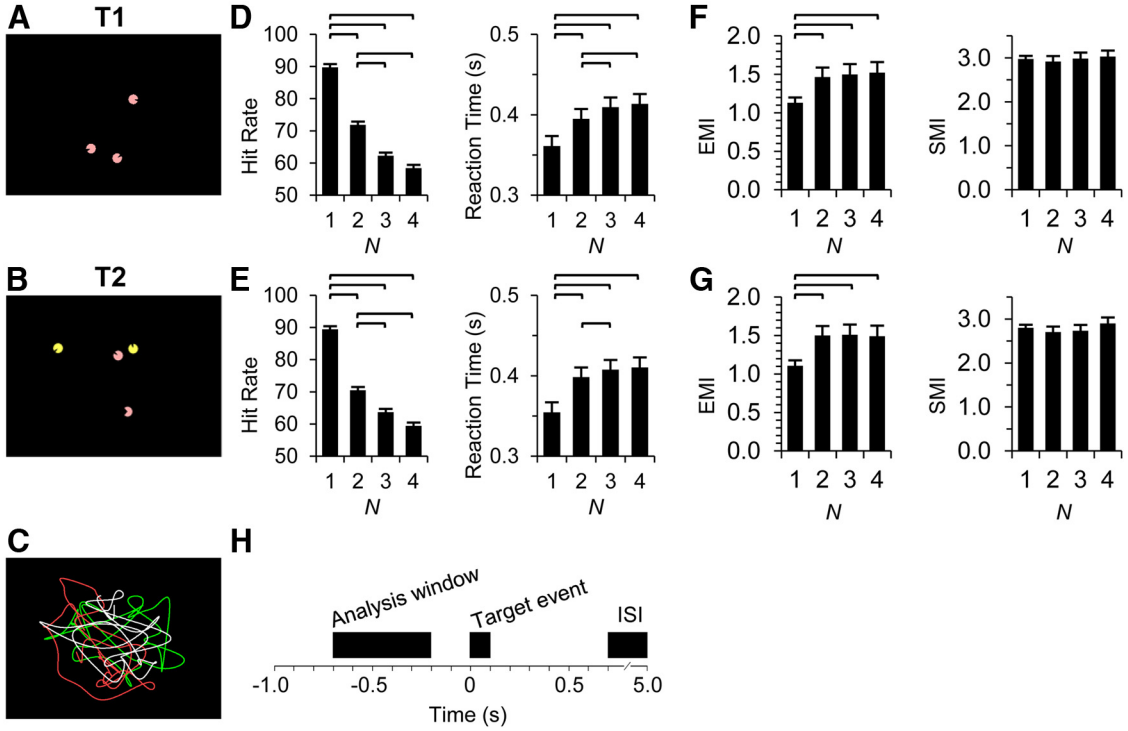

Figure 1. Experimental design and behavioral performance. ***A***, In T1, the subjects were instructed to attend one to four moving pink discs and to detect brief (~100 ms) changes in their shape (mouth openings). The example video frame is from a three-object condition. ***B***, In T2, the subjects attended only the pink discs and ignored the yellow. The number of discs presented was always four, whereas the number of attended pink discs varied from one to four. Here, the example is from a two-object condition with the object in bottom exhibiting the shape during the target event. ***C***, An example of paths along which the objects moved. ***D***, ***E***, The HRs and RTs decreased with an increasing number of attended objects in both T1 (***D***) and T2 (***E***). ***F***, ***G***, The overall magnitude of eye movements and the magnitude of fast (saccadic) movements were quantified with eye motion index (EMI) and saccade motion index (SMI), respectively. ***H***, A schematic of the analysis design. Time window used for the analyses of oscillation amplitudes was 700–200 ms before the occurrence of target events. The horizontal lines indicate significantly different pairs ($p < 0.05$, Bonferroni corrected, $N = 6$). Error bars indicate SEM.

equal amounts of trials from 2- and 3-target conditions, sorted the trials into four RT quartiles, and estimated across subjects whether intraquartile-mean oscillation amplitudes had a non-zero trend with a Pearson product moment correlation with a significance threshold of $p < 0.05$. To compare parametrically the amplitude modulations across attentional loads 2, 3, and 4, we used the Pearson product-moment correlation coefficient with significance threshold of $p < 0.05$ (see Figs. 3 and 4). For the division of subjects by capacity in Figure 4, we ordered the subjects by their mean capacity (see below) in the 4-target condition of T1 and T2 into high-capacity and low-capacity groups. To have an estimate of the significance of the group effect, we assessed the interaction term in a two-way ANOVA with capacity group and load as the factors ($p < 0.05$). We then estimated the Pearson product-moment correlation as in Figure 3 separately for each group ($p < 0.05$). To correlate individual attentional capacity with load-dependent amplitude modulations (see Fig. 5), we defined the capacity in each load condition ($N = 2$, 3, or 4 targets) as $C_i = N_i * Acc_i$, where C denotes capacity, Acc the target detection accuracy, and i the load condition. For each individual, these capacity values were detrended with the population mean, set individually to have a zero mean, and normalized to a unit area across the population. This approach yields a behavioral regressand where high-capacity subjects have a positive slope and low-capacity subjects a negative slope. By using oscillation amplitude data for the same N and with an identical normalization procedure, the null-hypothesis for a neuronal versus behavioral data is that the correlation coefficient is indistinguishable from zero. In Figure 5, positive correlations hence indicate that oscillation amplitudes are load-dependently strengthened more for the high- than for the low-capacity subjects and vice versa for the negative correlations. To compare task differences at separate target load conditions, we used t tests with significance threshold of $p < 0.05$ (see Fig. 6). To summarize the main results into a representative anatomic figure (Fig. 7), we plotted the total fraction of positive significance in the load and capacity conditions (Figs. 3 and 5). To account for multiple comparisons, statistical tests in each analysis were false discovery rate (FDR) corrected at the same time across the 400 brain regions in the anatomic parcellation and all 31 frequency bands (Palva et al., 2010, 2011).

Results

Behavioral performance

To examine the neuronal correlates of sustained attention, we used MOT tasks, in which the subjects were required to track one to four objects concurrently. The perceptual and attentional tracking performance was monitored by the subjects' responses to brief object shape changes. Example frames of the videos used in the experimental tasks are displayed in Figure 1*A*, *B*. In the first task (T1; Fig. 1*A*), the subjects tracked one to four discs that were moving in random, smooth curvilinear paths (Fig. 1*C*). Similarly to natural motion, the object velocity had a power–law relationship with path curvature so that the objects moved faster on the straighter parts and slower on tighter turns (Dayan et al., 2007). The subjects' task was to detect brief (~100 ms) changes in the object shape ("mouth openings") that presumably required the binding of object features. These target events were so brief that the subject could not scan the screen with saccades to improve performance or to "have a second glimpse" on any object to detect them. In the second task (T2; Fig. 1*B*), the task was otherwise the same, but to maintain a constant level of physical visual stimulation, the number of moving discs was always held at four and the subject was instructed to attend the pink discs and to ignore the yellow discs. The number of the attended discs varied again from one to four.

The target-event detection HRs decreased and the RTs increased as a function of the number of attended objects (Fig. 1*D*,*E*) so that the greatest change was between single-object and multiobject (2–4) tasks. This decrease in HR and increase in RT between single and multiobject conditions were also accompanied by an increase in the overall magnitude of eye movements in both tasks as indexed by the eye motion index (see Materials and Methods) ($p < 0.05$) but not in rapid saccade-like shifts in either task as indexed with the saccadic motion index ($p > 0.05$) (Fig. 1*F*,*G*). Importantly, the eye movements were not significantly different between 2-, 3-, and 4-object conditions in either of the tasks. Both the HRs ($p > 0.1$) and RTs ($p > 0.6$) were very similar between the two tasks, which indicates that the to-be-ignored stimuli in T2 did not affect the behavioral performance and suggests that T1 and T2 were close to each other in difficulty.

Pre-event oscillation amplitudes predict target detection

Our first aim was to investigate whether the strength of oscillation amplitudes could predict the subsequent detection of target events. Throughout this study, we used a time window from 700 to 200 ms before to target onset to probe the predictive value of neuronal oscillation amplitudes on behavioral performance (Fig. 1*H*). This window yielded ongoing task-state neuronal activity free of motor responses to prior targets, of neuronal responses evoked and induced by targets, and of blinks and large saccades. Because attention was sustained throughout the video presentations, this approach was expected to reveal those cortical regions of which the activity was modulated by changes in attentional and multiplexing task demands, and/or correlated with the success in the detection of the impending target event. In both tasks, successful task performance demanded multiplexing (i.e., the maintenance of multiple objects concurrently in the focus of attention but the two tasks differed in their requirements for selective attention). In T1, the increase in the number of attended objects conceivably increased attentional demands but also the total amount of physical visual input. Importantly, as in several prior visual WM (VWM) experiments, the increase in VWM load has been directly associated with the increase in visual load, this task provides an important link between attentional and WM studies. On the other hand, T2 reveals pure load-dependent attentional modulation because the physical stimulation remains the same across load conditions and, as evidenced by the lack of behavioral performance differences between T1 and T2, ignoring the distracters did not require significant or competing attentional resources.

In all analyses, the amplitudes were averaged across this window and the analysis-specific 2-, 3-, and/or 4-target trials among which we did not observe significant changes in eye movements (Fig. 1*F*,*G*). We first compared the oscillation amplitudes preceding detected and undetected target events and pooled the same amount of trials across 2- and 3-object conditions (see Materials and Methods). In both T1 (Fig. 2*A*; *t* test, $p < 0.05$, FDR-corrected) and T2 (Fig. 2*C*; *t* test, $p < 0.05$, FDR-corrected), the amplitudes of θ-oscillations (3–6.5 Hz) were negatively correlated with subsequent performance so that, on average, smaller amplitudes predicted better target detection performance. In addition, in T1, also the suppression of β-band amplitudes, and in T2, the suppression of α-amplitudes, predicted the subsequent detection of target events. In T1, the θ-band amplitude suppression was localized to anterior and posterior cingulate, insula, and precuneus as well as to early visual regions. It should be noted that, although the activity time series of superficial cortical areas can be reconstructed with good fidelity, the reconstruction of signals forms deep cortical structures, such as the cingulate, insula, and precuneus, and is less accurate and involves more signal mixing from nearby regions. The β-band amplitude suppression was observed only in the junction of the posterior inferior frontal sulcus and inferior precentral sulcus (Fig. 2*B*). In T2, the θ-/α-band amplitude suppression originated from precuneus and distributed visual regions. Importantly, the α- and β-band amplitudes were negatively correlated with target detection in distributed visual regions, inferior frontal sulcus, superior temporal gyrus, and insula (Fig. 2*D*).

Reaction times are correlated with prestimulus amplitude modulations

We next evaluated whether the strength of pretarget oscillation amplitudes would, in addition to biasing detection accuracy, have predictive value also for the RTs to the detected target events. We sorted the trials of 2- and 3-target conditions according to the RT quartiles into four equally large categories and then evaluated the correlation between mean RTs and mean oscillation amplitudes across these categories with the Pearson product-moment correlation test. The amplitudes of θ-, β-, and γ-band amplitudes were correlated negatively with RTs in T1 (Fig. 2*E*), whereas the β- and γ-amplitudes were correlated positively with RTs in T2 (Fig. 2*G*). The negative correlation here indicates that large-amplitude pretarget oscillations were associated with the longest post-target RTs, whereas a positive correlation indicates that they were associated with the fastest reactions. The negative correlations in θ-, β-, and γ-band amplitudes in T1 were observed in widely distributed cortical areas, including the sensorimotor cortex (SM) and LPFC and in the θ-band also in PPC in which intriguingly also a positive correlation was observed in the γ-band (Fig. 2*F*). On the other hand, the positive correlation with the β- and γ-band amplitudes and RTs were observed in distributed visual regions in extrastriate visual and temporal cortices as well as in LPFC specifically in the β-band.

Oscillation amplitudes are correlated with attentional load

To identify whether oscillation amplitudes would be modulated by the attention load as well as to identify the neuronal sources underlying these effects, we investigated the correlation of oscillation amplitudes with attentional load using the Pearson product-moment correlation test and 2-, 3-, and 4-object conditions. Because eye movements did not show significant trends in this range, and residual ocular signals were removed with ICA (see Materials and Methods), they were not a major confounder in the present analyses. In T1, an increasing attentional load was correlated with decreasing amplitudes of, α- and β-band oscillations and an increase in amplitudes in the γ-band (30–90 Hz; Fig. 3*A*). The load-dependent amplitude suppression was observed in the large parts of the PPC and occipital cortex (OC) (Fig. 3*B*), as well as in the temporoparietal junction (TPJ), superior parietal gyrus (SPG), inferior parietal gyrus (IPG), FEF, and anterior cingulate. In T2, we observed a similar, although weaker, load-dependent suppression of θ- to β-band amplitudes and a load-dependent increase in the amplitudes of β- and γ-band oscillations (Fig. 3*C*). In T2, the load-dependent amplitude suppression was observed in distributed areas of LPFC, SM, and FEF (Fig. 3*D*). Importantly, in both tasks, γ-band amplitudes were increased in LPFC, PPC, TPJ, cingulo-opercular (CO), and visual regions, and in T1 also in FEF and thus encompassed all task-relevant cortical regions in attentional processing (Kastner and Ungerleider, 2000). In addition to these presumably task-relevant cortical regions, γ-amplitudes were load-dependently

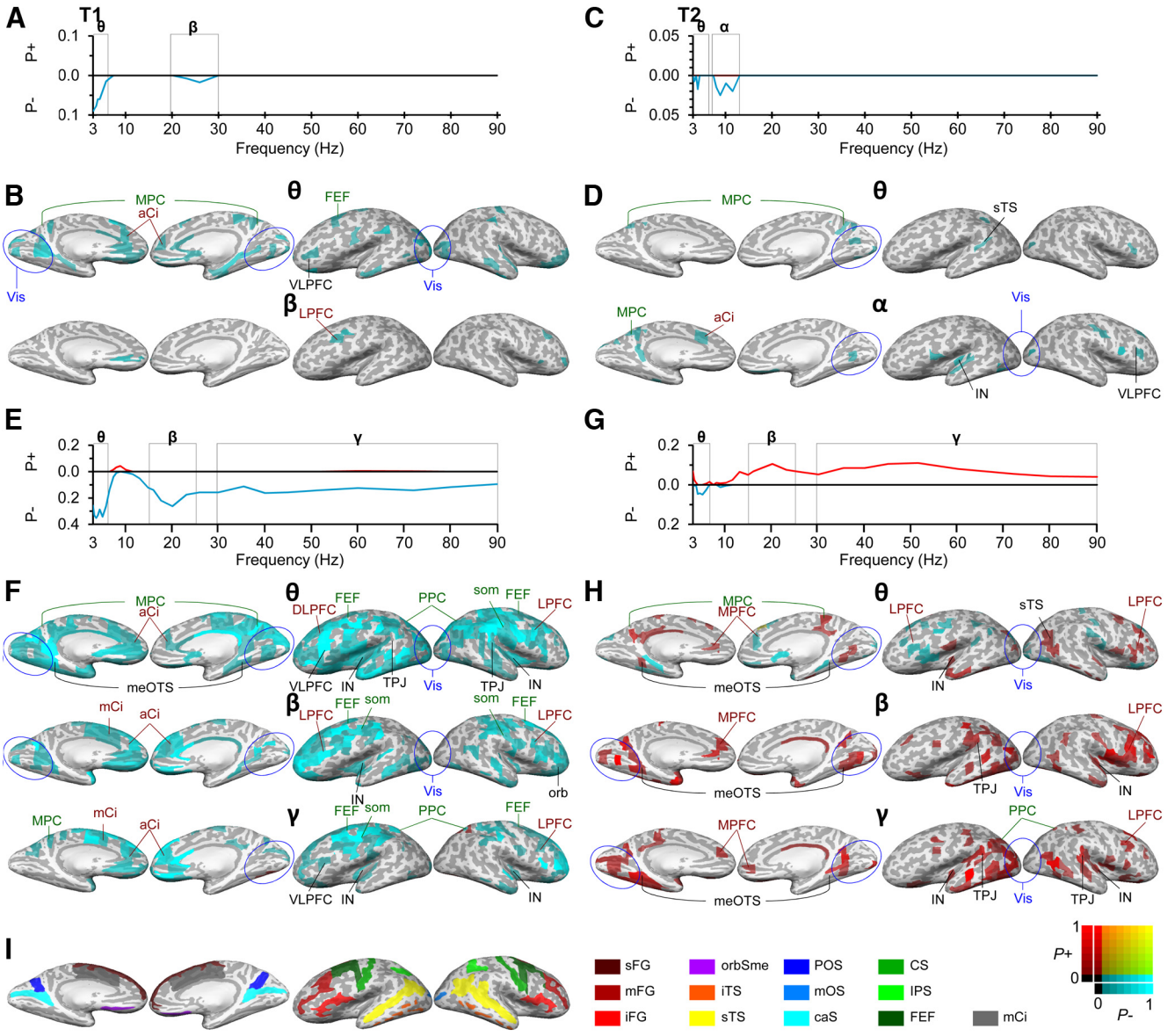

Figure 2. Oscillation amplitude modulations are correlated with target detection and RT. ***A***, In T1, detected target events were preceded by smaller oscillation amplitudes in θ- and β-bands than the missed target events. The *y*-axis displays the fraction of brain regions that had significantly larger (P^+) or smaller (P^-) mean oscillation amplitudes between the trials with correctly detected and missed target events. ***B***, The oscillation amplitudes in the α-band were decreased in distributed occipital, frontal, and temporal regions and medial cortical regions. Amplitudes are displayed in inflated cortical surface from a medial (left) and lateral (right) views. The color scale shows the fractions of negative (blue, P^-) and positive (red, P^+) significant observations in the frequency band of interest (see color scale in lower right corner). ***C***, In T2, detected targets were preceded by smaller oscillation amplitudes in θ- and α-bands than undetected targets. ***D***, Amplitude suppression was observed in the cingulate, insula, and visual cortical regions in OC and TC. ***E***, In T1, oscillation amplitudes are correlated negatively with the RTs in θ-, β-, and γ-bands, hence indicating that stronger amplitudes predicted slower performance (greater RTs). ***F***, Negative correlations with amplitudes and RTs were observed in SM regions, LPFC, including FEFs as well as in the medial cortical regions in cingulate and insula. The color scale indicates the fractions of significant positive and negative correlations. ***G***, In T2, oscillation amplitudes were correlated positively with the RTs in β- and γ-bands, indicating that greater pretarget amplitudes predicted faster performance (smaller RTs). ***H***, Positive correlations of oscillation amplitudes and RTs were observed across visual regions in OC, TC, and in PPC. ***I***, Colored landmark labels. A, Anterior; m, middle; p, posterior; s, superior; i, inferior; C, central; D, dorsal; F, frontal; G, gyrus; J, junction; L, lateral; M, medial; O, occipital; P, parietal; S, sulcus; T, temporal; V, ventral; caS, calcarine sulcus; Ci, cingulated; FEF, frontal eye field (putative); IN, insula; IPS, intraparietal sulcus and transparietal; orb, orbital; orbSme, orbital sulcus and medial olfactory; som, somatomotor; PC, parietal cortex; PFC, prefrontal cortex; PPC, posterior parietal cortex (includes intraparietal sulcus [IPS] and superior parietal gyrus [sPG]); Vis, early visual areas (~V1–V4, blue circle).

strengthened also in medial cortical structures. Together, load-dependent low-frequency amplitude suppression was observed in approximately overlapping regions to those showing load-dependent γ-amplitude increase.

Attentional load effects on oscillation amplitudes are distinct between high- and low-capacity subjects

To address whether the correlation of oscillation amplitudes with attentional load was associated with interindividual variability in attentional capacities, we first divided the subjects into two groups by their mean attentional capacity in T1 and T2 (Fig. 4*A* and *D*, respectively; for details, see Materials and Methods). To our surprise, in T1, the high β- and γ-band amplitudes were load-dependently strengthened exclusively in the high-capacity and not in the low-capacity group (Fig. 4*B*; Pearson's r, $p < 0.05$, FDR-corrected). Two-way ANOVA of load versus group effect corroborated that this load dependence of amplitudes was indeed significantly different between the low- and high-capacity groups

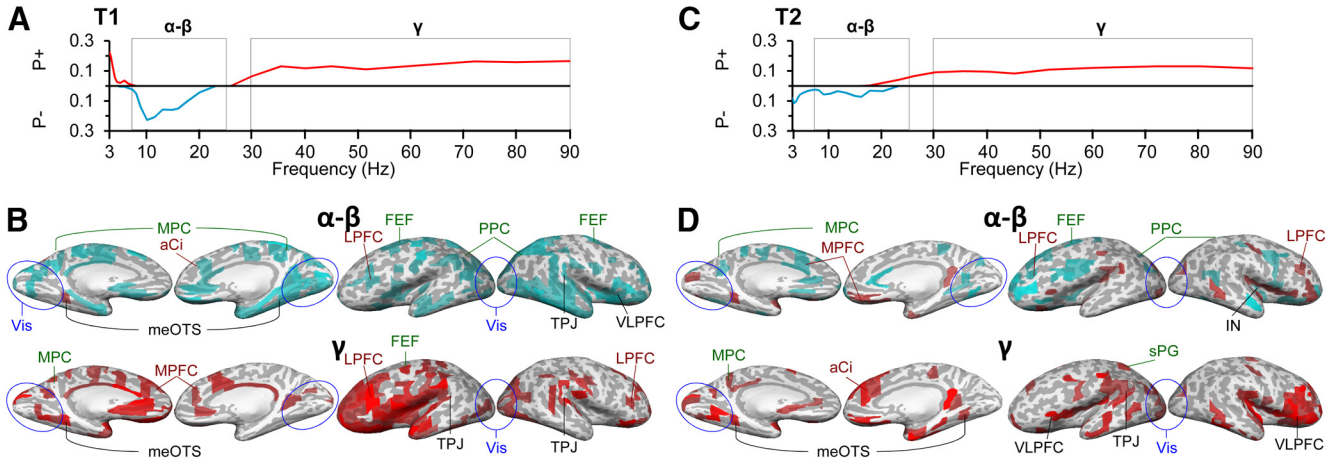

Figure 3. Attentional load modulates oscillation amplitudes similarly in T1 and T2. ***A***, In T1, increasing attentional load suppressed oscillation amplitudes in α- and β-bands and enhanced γ-band amplitudes. ***B***, Amplitudes were decreased in widespread OC, TC, and PC cortical regions but also in FEF, LPFC, and medial cortical structures. The color scale indicates the fractions of significant positive and negative correlations in the frequency bands of interest (Fig. 2). ***C***, In T2, attentional load strengthened oscillation amplitudes in the γ-band, whereas amplitudes in the α and β bands were only slightly suppressed. ***D***, Oscillation amplitudes in the γ-band were strengthened extensively in the ventral LPFC and also in PPC, TPJ, and cingulate. See Figure 2 for abbreviations.

(Fig. 4*B*). In addition, in high-capacity subjects, the load-dependent suppression peaked in the α-band, whereas in the low-capacity subjects it peaked in the β-band. The α-band suppression in high-capacity subjects was prominent over OC, PPC, SM, insula, and cingulate (Fig. 4*C*). The β-band suppression in low-capacity subjects was again prominent in cingulate and insula but observed also in PPC (in IPG and SPG). The positive correlations of γ-band amplitudes with attentional load in the high-capacity subjects were most prominent in OC, TC, and throughout the LPFC, including both the ventral (inferior) and dorsal (middle and superior) parts of the LPFC and extending to the most anterior parts of the LPFC. Importantly, load dependence of γ-amplitudes in high-capacity subjects was also observed in FEF and PPC (in IPG). In addition to these presumably task-relevant cortical regions, the load-dependent γ-amplitude increases were also observed in anterior cingulate, insula, and orbitofrontal structures.

In T2, the γ-band amplitudes were positively correlated with attentional load in both the high- and low-capacity subject groups (Pearson's r, $p < 0.05$, FDR-corrected), although, as in T1, this effect was still significantly greater in the high-capacity subjects (two-way ANOVA, $p < 0.05$, FDR-corrected; Fig. 4*E*). In addition, both groups showed a slight load-dependent decrease in α- and β-bands that was localized: in cingulate, superior temporal gyrus (STG), FEF, and superior frontal sulcus (SFS) (Fig. 4*F*). Interestingly, in high-capacity subjects, the γ-band amplitudes were observed in LPFC specifically in middle and inferior frontal gyrus and in PPC, including SPG as well as in insula and SM. In low-capacity subjects, γ-band activity was prominent in visual regions, after central sulcus, insula, and orbital structures, and hence showed less load-dependent activity in LPFC and PPC compared with high-capacity subjects (Fig. 4*F*).

Individual load-dependent modulation of oscillation amplitudes predicts interindividual variability in the attentional capacity

To further corroborate the findings of the high- versus low-capacity subject group comparison and to rigorously evaluate whether the strength of load dependence of oscillation amplitudes is correlated with individual attentional capacity, we computed the correlation between group-normalized oscillation amplitudes and similarly normalized attentional capacity values in the 2-, 3-, and 4-object conditions (Fig. 5*A*,*D*; see Materials and Methods). In this approach, a positive correlation indicates that the load-dependent amplitude modulation is with increasing load progressively more positive in high- than in low-capacity subjects. Vice versa, a negative correlation indicates that load-dependent modulations are more positive (or less negative) for the low- than for high-capacity subjects. As expected in T1, β- and γ-band amplitudes were positively correlated with the individual attentional capacity (Fig. 5*B*; Pearson's r, $p < 0.01$, FDR-corrected) and hence showed that in high-capacity subjects β- and γ-band amplitudes were relatively more increased by the attentional load. In addition, θ-band amplitudes were positively and α-band amplitudes negatively correlated with the individual attentional capacity, thus confirming the result from Figure 4. The positive correlation with attentional capacity in the γ-band was observed mostly in extrastriate visual regions, STS, SPG, and TPJ (Fig. 5*C*). Again, as predicted by the earlier group comparison (Fig. 4*E*), in T2 the attentional capacity was positively correlated with oscillation amplitudes throughout the frequency spectrum (Fig. 5*E*). The positive correlations in the γ-band confirm that the load-dependent strengthening of γ-band amplitudes indeed systematically covaried with interindividual variability in attentional capacity. These positive correlations were observed both in lateral OC (LOC), including TPJ, intraparietal sulcus (IPS), SM, as well as throughout LPFC (Fig. 5*F*).

Selective attention increases amplitudes across frequencies

We estimated how the selective attention aspect of T2 influenced oscillation amplitudes compared with the general attention demands of T1. We observed that the amplitudes in all frequency bands were stronger for the T2 than T1 (Fig. 6*A*; task effect for two-way ANOVA of task × load, $p < 0.01$, FDR-corrected); the sign of the T2-T1 task effect was determined by separate *post hoc* t tests (data not shown) in OC, TC, and LPFC (Fig. 6*B*). Because the behavioral performance was similar in T1 and T2 (Fig. 1), this effect was not the result of differences in task difficulty.

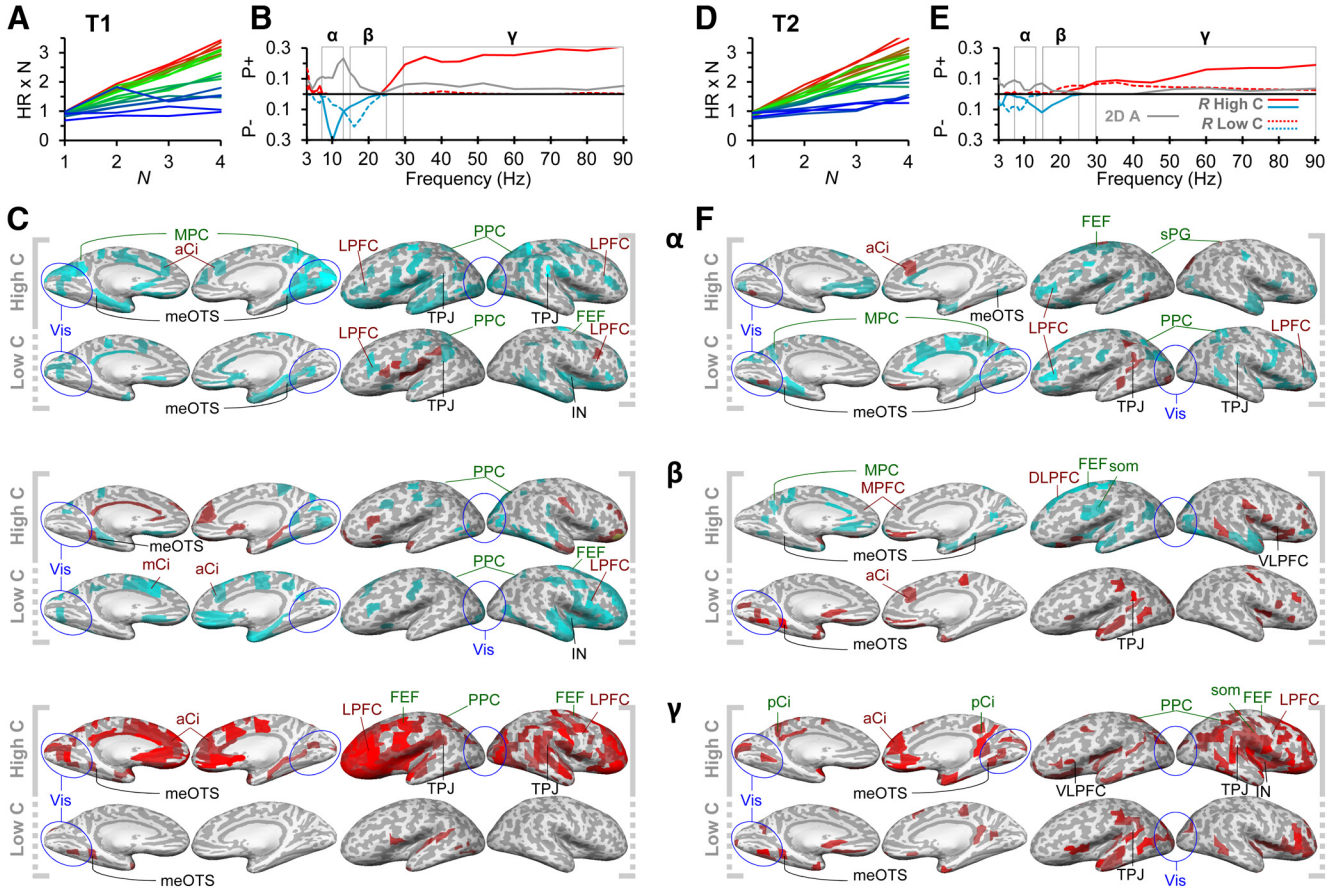

Figure 4. Attentional load modulates oscillation amplitudes differently in high- and low-capacity subjects. ***A***, Individual capacity values in T1 for each subject and load condition were obtained by multiplying the target detection accuracy (HR) with the number of attended objects. The *x*-axis denotes the number of attended objects (*N*) (i.e., the attentional load). Red represents subjects with highest mean capacity in T1 and T2; blue represents those with lowest capacity. The values were used to divide the subjects into high-capacity (warmer colors) and low-capacity subjects (colder colors) (see Materials and Methods). ***B***, In T1, attentional load strengthened γ-band amplitudes for high-capacity (solid lines) but not for low-capacity (dashed lines) subjects and suppressed the α- and β-band amplitudes differentially for high- and low-capacity subjects, respectively (Pearson's $r < 0.01$, FDR-corrected). These differences between groups were largely significant (gray line: two-way ANOVA, group × load interaction, $p < 0.05$, FDR-corrected). ***C***, In high-capacity subjects, γ-band amplitudes were strengthened in the visual regions in OC, TC, LPFC, as well as in cingulate and orbital areas, whereas in the low-capacity subject group, these load-dependent modulations were absent. Amplitude suppression in α- and β-bands was observed in distributed areas in PPC, LPFC, and in medial cortical structures as in cingulate and insula. The color scale is as in Figure 2. ***D***, Individual capacity values for T2 with the same subject-specific colors as in ***A***. ***E***, In T2, attentional load increased γ-band amplitudes both in high- and low-capacity subject groups (Pearson's $r < 0.01$, FDR-corrected), although the modulation was greater in the high-capacity subjects (two-way ANOVA, group × load interaction, $p < 0.05$, FDR-corrected) and decreased slightly α- and β-band amplitudes. ***F***, In low-capacity subjects, α-band suppression was observed in medial cortical structures specifically in cingulate in which the amplitude suppression in high-capacity subjects was not as pronounced. In both low- and high-capacity subjects, γ-band amplitudes were load-dependently strengthened in the LPFC.

Frontal, parietal, and visual regions underlie the distinct functions in multiobject attention

To summarize the variety of findings of this study, we overlaid the findings from both conditions and across different analyses. This summary revealed clusters of cortical regions underlying the correlations with multiobject attention and revealed most pronounced correlations in LPFC, SM, PPC, TPJ, and early visual regions (Fig. 7). To summarize and clarify the functional significance of these regions in multiobject attention, we plotted the mean Pearson correlation coefficients (load, capacity, and reaction time analyses) or relative amplitude values (*t*-test) within these ROIs as a function of frequency. This approach revealed that visual regions were correlated with detection accuracy and the number of attended object but much less with individual capacity. In contrast, β- and γ-oscillations were strongly correlated with individual attentional capacity in TPJ, PPC, SM, and LPFC, thus in regions higher in the visual processing hierarchy, although the β- and γ-band amplitudes correlated with the number of attended objects also in early visual regions. Detection accuracy, on the other hand, was positively correlated with α-amplitudes in PPC and γ-amplitudes in TPJ and early visual regions, but not with the oscillations in LPFC or SM. Similarly, oscillation amplitudes from α- to γ-bands in early visual regions and TPJ were correlated positively with RTs. Hence, oscillation amplitudes in early and late regions of visual processing hierarchy are differentially correlated with physical and mental processing stages of attended information, respectively.

Discussion

We used source-reconstructed MEG/EEG to address the functional role of human cortical oscillations in attention to multiple visual objects. We found that load-dependent suppression of θ-, α-, and low β-oscillations and strengthening of high β- and γ-oscillations in PPC, LPFC, and CO systems were the primary neuronal correlates of increasing attentional load. The present study extends prior observations on the relationship of γ oscillations and single-object attention in monkey local field potential and human MEG/EEG recordings on three fronts. The results

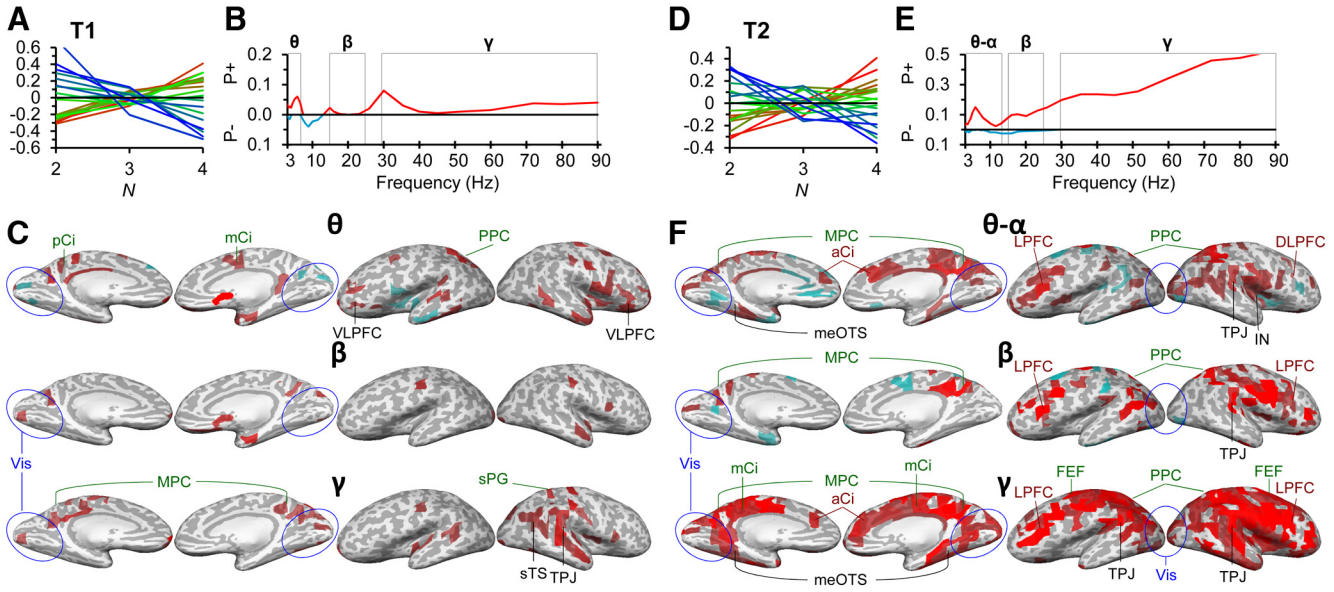

Figure 5. Attentional load-dependent modulation of γ-band amplitudes is correlated with individual attentional capacity. ***A***, Individual capacity values in T1 (see Fig. 4*A*) were used as the regressand in a correlation analysis after detrending with population mean performance, individual zero-meaning, and normalization to unit area under curve at the population level (see Materials and Methods). The *y*-axis displays the normalized capacity values. ***B***, In T1, θ- and α-band suppression and the strengthening of β- and γ-band amplitudes with attentional load were correlated with individual attentional capacity. ***C***, The load-dependently strengthened γ-band amplitudes were correlated with individual capacity limitations in several visual cortical regions in OC, TC, and PPC but also in distributed regions of LPFC and in cingulate and insula. ***D***, Normalized capacity values for T2 as in ***A***. ***E***, In T2, load-dependent increase in oscillation amplitudes in all frequency bands was correlated positively with individual capacity. ***F***, In θ–α-bands, positive correlations originated mainly from distributed visual regions in OC and TC and from PPC. In β- and γ-bands, the correlations between attentional capacity and load-dependent modulations were also observed in SM and throughout the LPFC.

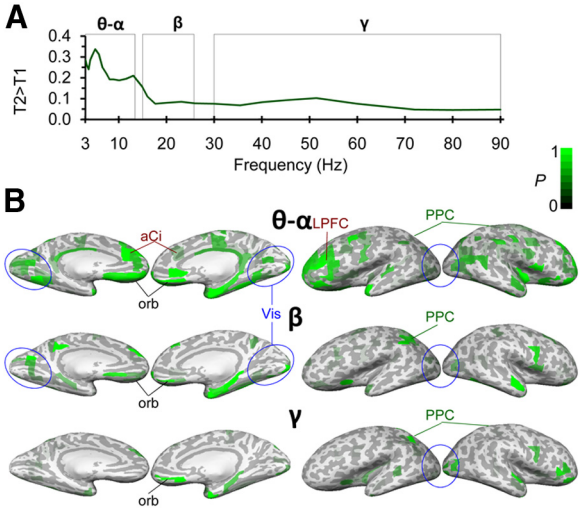

Figure 6. Oscillation amplitudes are greater in T2 than in T1 in all frequency bands. ***A***, T2 was associated with stronger oscillation amplitudes than T1 (task effect of the two-way ANOVA for task × load $p < 0.01$, FDR-corrected). ***B***, The stronger amplitudes in T2 originated from distributed visual regions mainly in temporal cortices as well as from distributed regions in LPFC.

show that multiobject attention is associated with progressive recruitment of γ-band activity, that these γ oscillations reflect the individual attentional capacity, and that the sources of these oscillations are not only those LPFC and CO regions that have been previously observed in fMRI recordings to be correlated with multiobject attentional demands (Kastner and Ungerleider, 2000; Jovicich et al., 2001), but also early visual regions. Together with prior data suggesting a mechanistic role for both α and γ oscillations in single-object attention (Palva and Palva, 2007; Womelsdorf and Fries, 2007; Siegel et al., 2008; Jensen and Mazaheri, 2010), these data thus suggest that single-object and multiobject attention may rely on partially overlapping neuronal mechanisms and cortical substrates.

Antagonistic pretarget θ-β and β-γ oscillations predict the success and speed of target detection

We first asked whether pretarget amplitude levels were correlated with the successful detection of target events and whether their strength was predictive of RTs. Intriguingly, in both tasks, only the suppression of low-frequency amplitudes was correlated with detection performance. The θ-, α-, and β-band suppressions were localized not only to early visual regions but also to LPFC, anterior cingulate, and insula (Fig. 2*B*,*D*) that belong to frontoparietal (FP) and CO task control networks (Dosenbach et al., 2008; Sadaghiani et al., 2010; Power et al., 2011). Prior data suggest that α-band amplitudes in sensory cortices are inversely correlated with cortical excitability (Mazaheri and Jensen, 2006; Klimesch et al., 2007; Romei et al., 2008; Lange et al., 2013). In spatial attention tasks, α-band amplitudes are enhanced in putatively task-irrelevant and/or unattended regions and suppressed in those where the attention is directed and task-relevant processing is performed (Worden et al., 2000). In MOT tasks, visual regions and LPFC (Culham et al., 1998; Jovicich et al., 2001) are likely to support task-oriented sensory and attentional processing, respectively (Raichle et al., 2001; Corbetta and Shulman, 2002; Power et al., 2011). The observed behavioral benefit from small-amplitude α oscillations in T2 in visual and lateral frontal task-relevant regions is thus in line with prevailing views. However, the observation of a similar effect in θ and β bands in T1 as well as the presence of amplitude suppression in CO network implies that the role of α amplitude in cortical excitability is more complex (Bollimunta et al., 2011; Mo et al., 2011; Lange et al., 2013).

Prior studies have shown that the strength of γ oscillations in OC (Hoogenboom et al., 2010) and FP (Gonzalez Andino et al., 2005) is correlated with RT in visual change detection so that

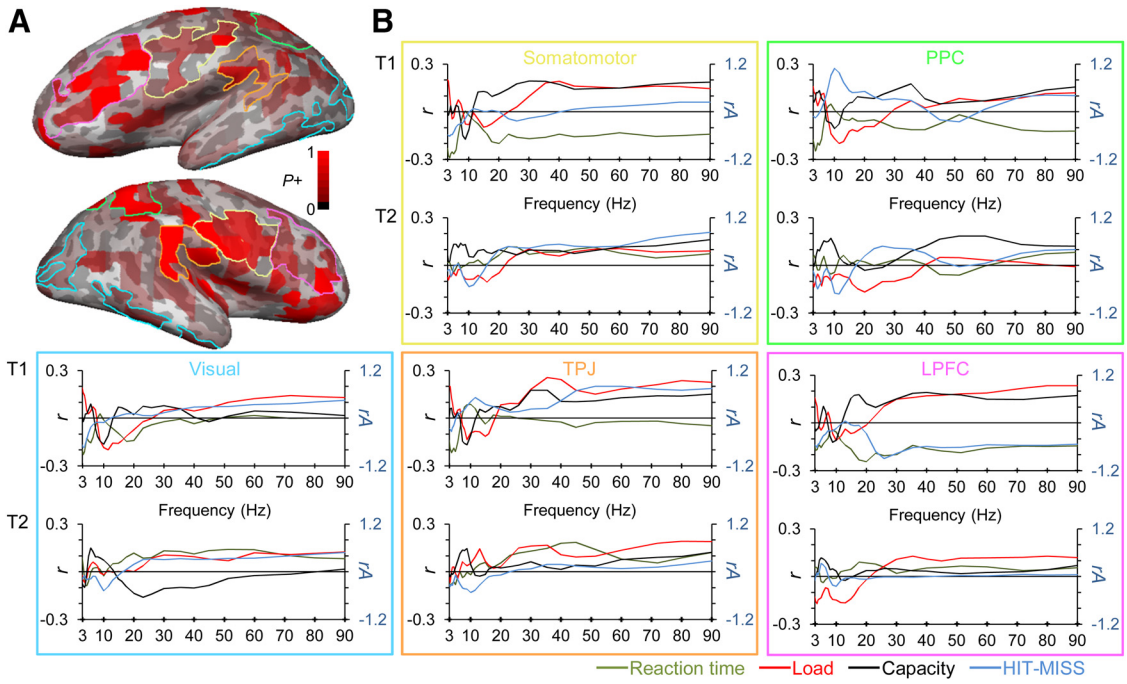

Figure 7. Summary of the main results reveals that oscillation amplitudes are differentially modulated by task demands in early and late regions of visual processing hierarchy. ***A***, Total fraction of positive significance in load and capacity conditions (Figs. 3 and 5) shown in inflated cortical surface. Pink, yellow, green, orange, and blue lines indicate LPFC, somatomotor (SM), PPC, TPJ, and visual ROIs, respectively. ***B***, Pearson correlation coefficients (*r*) for the correlation of oscillation amplitudes with load, capacity, and decreasing reaction time (red, black, and green lines). Blue lines denote the difference of relative oscillation amplitudes (*rA*) between detected and undetected trials.

stronger amplitudes predict shorter RTs. In line with these findings, we observed that stronger pretarget β- and γ-oscillations in T2 in OC and FP predicted shorter RTs. However, in T1, the opposite was observed in anterior LPFC where stronger pretarget β- and γ-band oscillations predicted longer RTs. This suggests that the engagement of higher-level attentional control regions slows behavioral performance.

Interestingly, whereas the pretarget oscillations from θ to γ bands were predictive of RT to target events, the γ oscillations apparently did not bias target detection per se. Slow and fast neuronal oscillations may hence have complementary attentional and representational functions in visual perception and attention (Singer, 1999; Klimesch et al., 2007; Palva and Palva, 2007; Womelsdorf and Fries, 2007).

γ oscillations are positively correlated with attentional load

In both tasks, the amplitude of prefrontal γ oscillations extending to the most anterior parts of the LPFC was positively correlated with attentional load. Widespread load-dependent increases in both low- and high γ-band amplitudes were observed in FEF, PPC, anterior cingulate, and insula as well as in visual regions. Attentional load thus modulated the γ-band amplitudes in cortical regions observed earlier in fMRI MOT studies (Culham et al., 1998; Jovicich et al., 2001) and belonging to FP and CO task-control systems (Corbetta and Shulman, 2002; Power et al., 2011). This result is significant as prior studies have shown that the strength of γ oscillations is correlated with attentional demands in monkeys (Womelsdorf et al., 2006; Gregoriou et al., 2009; Buschman and Miller, 2010; Bosman et al., 2012) and humans (Gruber et al., 1999; Siegel et al., 2008; Wyart and Tallon-Baudry, 2008), but the cortical loci of this phenomenon in humans have not been well characterized, and the role of γ oscillations in multiobject attention has remained unclear. LPFC, and specifically FEF, underlies the attentional top-down modulation of visual processing (Kastner and Ungerleider, 2000; Fuster, 2001; Buschman and Miller, 2007), whereas the anterior parts of LPFC are critical for higher-level cognitive operations when processing has to be integrated over time (Fuster, 2001, 2008). Importantly, as in a prior VWM MEG/EEG study (Palva et al., 2011), we observed here load-dependent β- and γ-band amplitude modulations in visual regions in addition to LPFC, although load-dependent activity in visual regions is not prominent in fMRI either for multiobject attention (Jovicich et al., 2001) or VWM (Linden et al., 2003). This may be attributed to the concurrent pronounced suppression of low-frequency activity in posterior structures. MEG and EEG may thus complement fMRI not only by providing spectral and temporal information, but also by revealing the spectrally limited participation of cortical regions not giving rise to net positive BOLD effects.

Load-dependent oscillations predict individual attentional capacity

To address the functional significance of the load-dependent γ oscillations, we assessed whether low- and high-capacity subjects exhibited distinct patterns of load dependence. The positive correlation of γ oscillations with attentional load in both T1 and T2 was stronger for the high- than for the low-capacity subjects (Fig. 4). This finding was corroborated both by a two-way ANOVA and an independent complementary analysis that investigated whether the load-dependent amplitude effects were directly correlated with the individual load-dependent decline in perceptual performance (Fig. 5). Both analyses showed that the load-dependent strengthening of γ oscillations in attentional FP and CO regions and OC, and occipito-temporal cortex that underlie visual processing (Riesenhuber and Poggio, 2002; Grill-Spector, 2003) was directly correlated with individual attentional capacity limits. Because the experimental parameters were constant across the population, these findings imply that the amplitude of γ os-

cillations reflects not the physical perceptual load but the number of perceptual objects maintained in the focus of attention. A similar association of γ synchronization with mental representations has been observed in other perceptual tasks, such as those involving masked words (Gaillard et al., 2009), visual grouping demands (Vidal et al., 2006), or a dissociation of the effects of awareness and attention on perceptual processing (Wyart and Tallon-Baudry, 2008). Moreover, a similar correlation with the load dependence of γ-band amplitudes and behavioral capacity was observed in a multiobject VWM study (Palva et al., 2011), which further supports the idea of common neuronal mechanisms underlying VWM and visual attention.

We observed positive correlations with individual capacity also in TPJ, PPC, and IPS. Electrocorticography has shown that γ oscillations in TPJ are critical for perception (Beauchamp et al., 2012), whereas IPS is a key region for VWM capacity in fMRI studies (Todd and Marois, 2004; Xu and Chun, 2006) and a central hub in synchronized interareal networks predicting VWM capacity (Palva et al., 2010). Given the notion that sensory features are bound into coherent object representations only when attended (Treisman and Gelade, 1980), the proposed role of γ synchronization in sensory feature binding (Singer, 1999), integrated neuronal object representations (Tallon-Baudry et al., 1998), and the role of IPS and superior parietal cortex in feature integration when multiple objects are attended (Shafritz et al., 2002), we propose that the posterior γ oscillations support the feature binding of the successfully attended objects. Our results also support the hypothesis that γ-band activity in FP networks imposes selective attentional top-down modulation of sensory processing (Womelsdorf and Fries, 2007; Gregoriou et al., 2009).

Oscillation amplitudes are correlated with the task set requirements

The comparison of T2 and T1 showed that the additional task demands on selective attention in T2 were associated with overall enhanced oscillation amplitudes. This effect was salient in widespread visual regions in the occipital and inferotemporal cortex, which is in line with the idea that selective attention operates by facilitating the processing in task-relevant sensory regions (Kastner and Ungerleider, 2000; Corbetta and Shulman, 2002) and that selective attention operates through neuronal synchronization (Womelsdorf and Fries, 2007). As the tasks were acquired in separate sessions, this difference is likely also related to task-set maintenance by the CO system (Dosenbach et al., 2008; Sadaghiani et al., 2010).

References

Beauchamp MS, Sun P, Baum SH, Tolias AS, Yoshor D (2012) Electrocorticography links human temporoparietal junction to visual perception. Nat Neurosci 15:957–959. CrossRef Medline

Bettencourt KC, Michalka SW, Somers DC (2011) Shared filtering processes link attentional and visual short-term memory capacity limits. J Vis 11:10. CrossRef Medline

Bollimunta A, Mo J, Schroeder CE, Ding M (2011) Neuronal mechanisms and attentional modulation of corticothalamic alpha oscillations. J Neurosci 31:4935–4943. CrossRef Medline

Bosman CA, Schoffelen JM, Brunet N, Oostenveld R, Bastos AM, Womelsdorf T, Rubehn B, Stieglitz T, De Weerd P, Fries P (2012) Attentional stimulus selection through selective synchronization between monkey visual areas. Neuron 75:875–888. CrossRef Medline

Buschman TJ, Miller EK (2007) Top-down versus bottom-up control of attention in the prefrontal and posterior parietal cortices. Science 315:1860–1862. CrossRef Medline

Buschman TJ, Miller EK (2010) Shifting the spotlight of attention: evidence for discrete computations in cognition. Front Hum Neurosci 4:194. CrossRef Medline

Corbetta M, Shulman GL (2002) Control of goal-directed and stimulus-driven attention in the brain. Nat Rev Neurosci 3:201–215. CrossRef Medline

Cowan N, Elliott EM, Scott Saults J, Morey CC, Mattox S, Hismjatullina A, Conway AR (2005) On the capacity of attention: its estimation and its role in working memory and cognitive aptitudes. Cogn Psychol 51:42–100. CrossRef Medline

Culham JC, Brandt SA, Cavanagh P, Kanwisher NG, Dale AM, Tootell RB (1998) Cortical fMRI activation produced by attentive tracking of moving targets. J Neurophysiol 80:2657–2670. Medline

Dale AM, Fischl B, Sereno MI (1999) Cortical surface-based analysis: I. Segmentation and surface reconstruction. Neuroimage 9:179–194. CrossRef Medline

Dayan E, Casile A, Levit-Binnun N, Giese MA, Hendler T, Flash T (2007) Neural representations of kinematic laws of motion: evidence for action-perception coupling. Proc Natl Acad Sci U S A 104:20582–20587. CrossRef Medline

Dosenbach NU, Fair DA, Cohen AL, Schlaggar BL, Petersen SE (2008) A dual-networks architecture of top-down control. Trends Cogn Sci 12:99–105. CrossRef Medline

Drew T, Vogel EK (2008) Neural measures of individual differences in selecting and tracking multiple moving objects. J Neurosci 28:4183–4191. CrossRef Medline

Fischl B, Sereno MI, Dale AM (1999) Cortical surface-based analysis: II. Inflation, flattening, and a surface-based coordinate system. Neuroimage 9:195–207. CrossRef Medline

Fischl B, Salat DH, Busa E, Albert M, Dieterich M, Haselgrove C, van der Kouwe A, Killiany R, Kennedy D, Klaveness S, Montillo A, Makris N, Rosen B, Dale AM (2002) Whole brain segmentation: automated labeling of neuroanatomical structures in the human brain. Neuron 33:341–355. CrossRef Medline

Fuster JM (2001) The prefrontal cortex—an update: time is of the essence. Neuron 30:319–333. CrossRef Medline

Fuster JM (2008) The prefrontal cortex. New York: Academic Elsevier.

Gaillard R, Dehaene S, Adam C, Clémenceau S, Hasboun D, Baulac M, Cohen L, Naccache L (2009) Converging intracranial markers of conscious access. PLoS Biol 7:e61. CrossRef Medline

Gonzalez Andino SL, Michel CM, Thut G, Landis T, Grave de Peralta R (2005) Prediction of response speed by anticipatory high-frequency (γ band) oscillations in the human brain. Hum Brain Mapp 24:50–58. CrossRef Medline

Gregoriou GG, Gotts SJ, Zhou H, Desimone R (2009) High-frequency, long-range coupling between prefrontal and visual cortex during attention. Science 324:1207–1210. CrossRef Medline

Grill-Spector K (2003) The neural basis of object perception. Curr Opin Neurobiol 13:159–166. CrossRef Medline

Gruber T, Müller MM, Keil A, Elbert T (1999) Selective visual-spatial attention alters induced gamma band responses in the human EEG. Clin Neurophysiol 110:2074–2085. CrossRef Medline

Hämäläinen MS, Ilmoniemi RJ (1994) Interpreting magnetic fields of the brain: minimum norm estimates. Med Biol Eng Comput 32:35–42. CrossRef Medline

Hämäläinen MS, Sarvas J (1989) Realistic conductivity geometry model of the human head for interpretation of neuromagnetic data. IEEE Trans Biomed Eng 36:165–171. CrossRef Medline

Hoogenboom N, Schoffelen JM, Oostenveld R, Fries P (2010) Visually induced gamma-band activity predicts speed of change detection in humans. Neuroimage 51:1162–1167. CrossRef Medline

Jensen O, Mazaheri A (2010) Shaping functional architecture by oscillatory α activity: gating by inhibition. Front Hum Neurosci 4:186. CrossRef Medline

Jovicich J, Peters RJ, Koch C, Braun J, Chang L, Ernst T (2001) Brain areas specific for attentional load in a motion-tracking task. J Cogn Neurosci 13:1048–1058. CrossRef Medline

Kastner S, Ungerleider LG (2000) Mechanisms of visual attention in the human cortex. Annu Rev Neurosci 23:315–341. CrossRef Medline

Klimesch W, Sauseng P, Hanslmayr S (2007) EEG α oscillations: the inhibition-timing hypothesis. Brain Res Rev 53:63–88. CrossRef Medline

Lange J, Oostenveld R, Fries P (2013) Reduced occipital α power indexes enhanced excitability rather than improved visual perception. J Neurosci 33:3212–3220. CrossRef Medline

Linden DE, Bittner RA, Muckli L, Waltz JA, Kriegeskorte N, Goebel R, Singer

W, Munk MH (2003) Cortical capacity constraints for visual working memory: dissociation of fMRI load effects in a fronto-parietal network. Neuroimage 20:1518–1530. CrossRef Medline

Luck SJ, Vogel EK (1997) The capacity of visual working memory for features and conjunctions. Nature 390:279–281. CrossRef Medline

Mazaheri A, Jensen O (2006) Posterior α activity is not phase-reset by visual stimuli. Proc Natl Acad Sci U S A 103:2948–2952. CrossRef Medline

Mo J, Schroeder CE, Ding M (2011) Attentional modulation of alpha oscillations in macaque inferotemporal cortex. J Neurosci 31:878–882. CrossRef Medline

Oksama L, Hyönä J (2004) Is multiple object tracking carried out automatically by an early vision mechanism independent of higher-order cognition? An individual difference approach. Vis Cogn 11:631–671. CrossRef

Palva JM, Monto S, Kulashekhar S, Palva S (2010) Neuronal synchrony reveals working memory networks and predicts individual memory capacity. Proc Natl Acad Sci U S A 107:7580–7585. CrossRef Medline

Palva S, Palva JM (2007) New vistas for α-frequency band oscillations. Trends Neurosci 30:150–158. CrossRef Medline

Palva S, Linkenkaer-Hansen K, Näätänen R, Palva JM (2005) Early neural correlates of conscious somatosensory perception. J Neurosci 25:5248–5258. CrossRef Medline

Palva S, Kulashekhar S, Hämäläinen M, Palva JM (2011) Localization of cortical phase and amplitude dynamics during visual working memory encoding and retention. J Neurosci 31:5013–5025. CrossRef Medline

Power JD, Cohen AL, Nelson SM, Wig GS, Barnes KA, Church JA, Vogel AC, Laumann TO, Miezin FM, Schlaggar BL, Petersen SE (2011) Functional network organization of the human brain. Neuron 72:665–678. CrossRef Medline

Pylyshyn ZW, Storm RW (1988) Tracking multiple independent targets: evidence for a parallel tracking mechanism. Spat Vis 3:179–197. CrossRef Medline

Raichle ME, MacLeod AM, Snyder AZ, Powers WJ, Gusnard DA, Shulman GL (2001) A default mode of brain function. Proc Natl Acad Sci U S A 98:676–682. CrossRef Medline

Riesenhuber M, Poggio T (2002) Neural mechanisms of object recognition. Curr Opin Neurobiol 12:162–168. CrossRef Medline

Romei V, Brodbeck V, Michel C, Amedi A, Pascual-Leone A, Thut G (2008) Spontaneous fluctuations in posterior alpha-band EEG activity reflect variability in excitability of human visual areas. Cereb Cortex 18:2010–2018. CrossRef Medline

Roux F, Wibral M, Mohr HM, Singer W, Uhlhaas PJ (2012) γ-band activity in human prefrontal cortex codes for the number of relevant items maintained in working memory. J Neurosci 32:12411–12420. CrossRef Medline

Saalmann YB, Pinsk MA, Wang L, Li X, Kastner S (2012) The pulvinar regulates information transmission between cortical areas based on attention demands. Science 337:753–756. CrossRef Medline

Sadaghiani S, Scheeringa R, Lehongre K, Morillon B, Giraud AL, Kleinschmidt A (2010) Intrinsic connectivity networks, α oscillations, and tonic alertness: a simultaneous electroencephalography/functional magnetic resonance imaging study. J Neurosci 30:10243–10250. CrossRef Medline

Shafritz KM, Gore JC, Marois R (2002) The role of the parietal cortex in visual feature binding. Proc Natl Acad Sci U S A 99:10917–10922. CrossRef Medline

Siegel M, Donner TH, Oostenveld R, Fries P, Engel AK (2008) Neuronal synchronization along the dorsal visual pathway reflects the focus of spatial attention. Neuron 60:709–719. CrossRef Medline

Singer W (1999) Neuronal synchrony: a versatile code for the definition of relations? Neuron 24:49–65, 111–125. CrossRef Medline

Tallon-Baudry C, Bertrand O, Delpuech C, Pernier J (1996) Stimulus specificity of phase-locked and non-phase-locked 40 Hz visual responses in human. J Neurosci 16:4240–4249. Medline

Tallon-Baudry C, Bertrand O, Peronnet F, Pernier J (1998) Induced γ-band activity during the delay of a visual short-term memory task in humans. J Neurosci 18:4244–4254. Medline

Todd JJ, Marois R (2004) Capacity limit of visual short-term memory in human posterior parietal cortex. Nature 428:751–754. CrossRef Medline

Treisman A (2006) How the deployment of attention determines what we see. Vis Cogn 14:411–443. CrossRef Medline

Treisman AM, Gelade G (1980) A feature-integration theory of attention. Cogn Psychol 12:97–136. CrossRef Medline

Vidal JR, Chaumon M, O'Regan JK, Tallon-Baudry C (2006) Visual grouping and the focusing of attention induce γ-band oscillations at different frequencies in human magnetoencephalogram signals. J Cogn Neurosci 18:1850–1862. CrossRef Medline

Vogel EK, Machizawa MG (2004) Neural activity predicts individual differences in visual working memory capacity. Nature 428:748–751. CrossRef Medline

Womelsdorf T, Fries P (2007) The role of neuronal synchronization in selective attention. Curr Opin Neurobiol 17:154–160. CrossRef Medline

Womelsdorf T, Fries P, Mitra PP, Desimone R (2006) γ-band synchronization in visual cortex predicts speed of change detection. Nature 439:733–736. CrossRef Medline

Worden MS, Foxe JJ, Wang N, Simpson GV (2000) Anticipatory biasing of visuospatial attention indexed by retinotopically specific α-band electroencephalography increases over occipital cortex. J Neurosci 20:RC63. Medline

Wyart V, Tallon-Baudry C (2008) Neural dissociation between visual awareness and spatial attention. J Neurosci 28:2667–2679. CrossRef Medline

Xu Y, Chun MM (2006) Dissociable neural mechanisms supporting visual short-term memory for objects. Nature 440:91–95. CrossRef Medline

Xu Y, Chun MM (2009) Selecting and perceiving multiple visual objects. Trends Cogn Sci 13:167–174. CrossRef Medline